Multi-day water residence time as a mechanism for physical and biological gradients across intertidal flats

Elizabeth E. Wheat[1], Neil S. Banas[2], Jennifer L. Ruesink[3]*

[1]Program on the Environment, University of Washington, Box 355679, Seattle, Washington, 98195-5679

[2]Department of Mathematics and Statistics, University of Strathclyde, Glasgow G1 1XQ, UK

[3]Department of Biology, University of Washington, Box 351800, Seattle, Washington, 98195-1800 USA

*Corresponding author: ruesink@u.washington.edu

Abstract

Tidal flats with shallow-sloping bathymetry under meso- to macrotidal conditions allow organisms to occupy similar tidal elevations at different distances from subtidal channels. As water floods or ebbs across such tidal flats during a single tidal cycle, upstream organisms may modify water properties such as chlorophyll concentration, while physiochemical properties may change due to close association with sediments. Here we report evidence for an additional mechanism establishing cross-shore gradients: multi-day water residence times, in the sense that even if water completely drains into subtidal channels at low tide, a large fraction returns to the flats on the next high tide. We applied circulation modeling and empirical measurements of water properties and benthic secondary production to a 1-km-wide tidal flat in Willapa Bay, Washington, USA. From the circulation model, water parcels on this intertidal flat have residence times up to 2 d, that is, water found on the flat at one high tide returns to the intertidal zone for a median of 4 successive semidiurnal high tides. Modeled residence times generally increased towards shore. Four empirical datasets showed cross-shore gradients consistent with modeled residence times: Salinity time series lagged towards shore; water column chlorophyll declined towards shore at fixed stations (near-bottom) and in surface transects more than could be explained by benthic suspension-feeding during a single transit of water; and oyster (*Magallana = Crassostrea gigas*) condition declined 25% over 0.5 km from channel to shore, independent of tidal elevation. One environmental measurement was more consistent with within-tide change, as water temperatures warmed towards shore on afternoon flood tides but showed no tidal-cycle lags. Taken together, these patterns suggest that multi-day water residence times can

contribute to environmental heterogeneity from channel to shore on tidal flats, acting orthogonally to well-recognized estuarine gradients in residence time from ocean to river.

Keywords: benthic suspension feeders; circulation model; Crassostrea gigas; intertidal gradients; residence time; water column chlorophyll

1 Introduction

Coastal-plain estuaries and tidal embayments typically show systematic variation in residence time and water age along the main axis from ocean mouth to head. The along-channel residence-time gradient, which summarizes the net effect of various circulation and mixing processes over a number of tidal cycles, broadly impacts biological and biogeochemical estuarine dynamics. Increased residence time increases the fraction of nitrogen that is denitrified (Dettmann, 2001), modifies sediment grain size (Wiberg et al., 2015), reduces larval dispersal (Abelson and Denny, 1997), and results in reductions of water column chlorophyll (Alpine and Cloern, 1992; Dame and Prins, 1998; Banas et al., 2007). In estuaries with broad intertidal areas, it is much less common to analyze cross-shore gradients (from the main channel to shore across a tidal flat) in terms of residence time, as opposed to other schemas like tidal elevation or wave exposure. One might well assume, in fact, that the residence time of the intertidal zone is, by definition, at most a few hours, between one flood tide and the next ebb, and therefore simply not commensurate with the multi-day residence times commonly seen on larger scales and in deeper water. This study combines observations in Willapa Bay, Washington, USA

with semi-idealized numerical modeling to present a counterexample, in which residence-time gradients provide a key mechanism for gradients in water properties and secondary production across an intertidal mudflat.

An earlier model of Willapa Bay (Banas and Hickey, 2005; Banas et al., 2007) predicted strong residence-time gradients orthogonal to the estuarine axis, but those studies did not have a means to validate that finding, or explore its biological implications. These gradients did not reflect zonation associated with tidal elevation, but rather a circulation pattern in which a large fraction of the water that ebbs off a flat into the main channel returns on the subsequent flood tide, and in which the fraction returned is greater for water found close to shore at high tide.

Such small-scale variation in residence time may influence the productivity of benthic organisms that depend on delivery of water column resources. Energy budgets for Pacific oysters (*Magallana = Crassostrea gigas* Thunberg), as well as statistical models relating oyster growth to environmental conditions, reveal strong effects of food resources (Ren and Ross, 2001; Gangnery et al., 2003), water flow (Lenihan et al., 1996), temperature, and salinity (Brown and Hartwick, 1988; Whyte et al., 1990; Ruiz et al., 1992). Food quantity changes dynamically as particle concentrations are reduced through grazing or increased through cell division or resuspension of benthic particles. At small scales, individual performance may thus decline as density of benthic suspension-feeders increases (Peterson and Black, 1987), and at larger scales those individuals that are downstream may experience lower particle concentrations because upstream individuals have already removed some (Grizzle et al., 2008).

Intertidal zonation in soft sediments is well established (Peterson, 1991; Dittman, 2000; Ryu et al., 2011), as is the effect of immersion time on performance within species (e.g. bivalves Ruesink et al., 2003; Bishop and Peterson, 2006; Tomiyama et al., 2010; Walles et al., 2016; Lomovasky et al., 2018). Yet in addition to the manifest ramifications of how long water covers a particular intertidal point, the properties of that water also shape the environmental context experienced by organisms. Thus an understanding of the circulation and retention of water on tidal flats, which may underlie heterogeneous water properties, becomes essential. An important distinction is illustrated conceptually in Fig. 1. For water crossing a tidal flat during a single incoming tide, water column resources may be filtered out during passage across beds of suspension-feeders, resulting in downstream individuals with lower resource availability (Fig. 1a). However, from a tidally-averaged perspective, some parcels of water may be influenced by benthic suspension-feeders over multiple tides, and those portions of the tidal flat with longer residence times may consequently have depleted water column resources (Fig. 1b).

In addition to enhancing gradients in some water properties through longer interactions with the benthos, water residence time on tidal flats has the potential to generate lags in conservative tracers. During summer conditions of low riverflow, especially at the mouth of Willapa Bay, salinity varies primarily due to the source water that is tidally advected from the ocean, with salinity rising during upwelling, and falling during downwelling (Roegner et al., 2002; Hickey et al., 2002; Ruesink et al., 2015). Overall, water that has experienced an extended residence time could therefore be higher or lower in salinity than “newer” water, depending on its origins during upwelling or

downwelling conditions. High residence time should consistently lead to warmer water in summer, due to solar heating of dark tidal flats (Harrison and Phizacklea, 1987; Hickey and Banas, 2003).

In this paper we contribute evidence that the retention of water over multiple tidal cycles, combined with the feeding activity of suspension-feeders, causes food limitation in the intertidal zone, thus affecting secondary production. Oyster growers respond to spatial variation in oyster growth at our study site by moving oysters in the intertidal zone from shore to channel for fattening (improved meat weight; Hedgpeth and Obrebski, 1981). Our focal questions were:

1) What is the pattern of water residence time across this intertidal flat based on circulation modeling?
2) Are channel-to-shore gradients in water properties (salinity, temperature, chlorophyll) consistent with an extended water residence time?
3) How variable are oyster growth and condition from channel to shore, controlling for tidal elevation?

The overall goal is therefore to evaluate a previously unexplored mechanism of intertidal water residence time in establishing cross-shore physical and biological gradients on tidal flats.

2 Methods

2.1 Study site

Willapa Bay, Washington, USA, has extensive tidal flats, with half of the bay area out of the water on extreme low tides. We selected a tidal flat to study near the bay mouth (46.59N, 124.02W, Fig. 2, 3), where much of the flat is occupied by commercial on-bottom oyster culture, supported by plankton blooms advected from the nearshore ocean (Roegner et al., 2002). Commercial shellfish aquaculture, primarily for Pacific oysters, occupies approximately 20% of Willapa Bay's intertidal area (Feldman et al., 2000), yielding up to 17% of the oysters cultured in the United States (Dumbauld and McCoy, 2015). Within ca. 50 ha at our study site, 38,000 bushels of oysters are harvested annually (F. Wiegardt, pers. comm.).

2.2 Circulation model of residence time

Banas and Hickey (2005) presented and validated a 255-m-resolution circulation model of Willapa Bay, run under a variety of tide, riverflow, and wind forcing conditions. More recently, a preliminary coupled bio-physio-chemical model of Willapa Bay, implemented in ROMS (Regional Ocean Modeling System: Haidvogel et al., 2008) at 500 m resolution, has been introduced as part of the LiveOcean system (https://faculty.washington.edu/pmacc/LO/LiveOcean.html) and is being used to produce daily forecasts. The model used in this study is a branch of the Banas and Hickey (2005) model, implemented in ROMS but independent of the LiveOcean project, and designed not for realistic hindcasting but for process insight, in the same spirit as a tabletop fluid-dynamical lab experiment. Compared with the original Banas and Hickey (2005) model, the ROMS model used here has simplified external forcing but, crucially, much higher spatial resolution (50 m) and updated intertidal bathymetry.

The base bathymetry used in the model is the same as that used by Banas and Hickey (2005), a dataset provided by the US Army Corps of Engineers Seattle District, based on a survey of Willapa Bay's subtidal channels in 1998 (Kraus, 2000). Into this model grid we substituted an improved intertidal bathymetric dataset, provided by the Olympic Natural Resources Center (ONRC), which merges NOAA Coastal Service Center LiDAR with locally collected point soundings and vertical datum transformations for integration with USGS National Hydrographic Datasets by the ONRC staff. The final model bathymetry uses the ONRC bathymetry at depths between 1.55 m above and 1.55 m below mean sea level (1.55 is the average of the difference between mean tide level and mean lower low water (MLLW) at 7 NOAA sites around the bay), and the Kraus (2000) model grid at deeper depths.

The model case used is a semi-idealized representation of summer, low-riverflow conditions, in which the circulation is forced only by the semidiurnal (M2) tide and its interaction with complex bathymetry, including wetting and drying of intertidal banks (Oey, 2005; Warner, 2010; Xue and Du, 2010). For efficiency and stability, this implementation of the model (unlike the original) is two-dimensional, i.e., barotropic: this allows us to resolve fine-scale bathymetry with less smoothing, although some flow information is lost. Banas et al. (2004) showed that neglecting baroclinic processes was a fair approximation for late-summer, low-riverflow conditions in Willapa Bay, although this simplification would not be appropriate for winter or spring conditions. M2 tidal amplitude at the open boundary was set at 1.2 m. This produces a standard deviation (SD) in sea level of 0.85 m at Toke Point near the bay mouth (NOAA station 9440910,

46° 42.5’ N, 123° 58’ W), which matches the observed SD of sea level at Toke Point over three years to within 1%.

Net circulation, residence time, and horizontal tidal diffusivity (a measure of the strength of tidal stirring and the residual, tidally-averaged circulation) were calculated based on the statistics of 170,000 particles (one per 50 m x 50 m grid cell) tracked for one tidal cycle using depth-averaged currents. Beginning and ending positions of the particles were used to construct a transition matrix or “tidal return map” (Banas and Hickey, 2005; Banas et al., 2009) from which longer trajectories and residence-time statistics were calculated. Residence times are reported below at 200 m resolution, based on clusters of 16 particles released with 50 m spacing. Residence time is here defined as the length of time that more than half of the 16 particles released in each 200 m square at high tide continue to be found in the intertidal zone at successive high tides (where each successive high tide in this calculation represents one set of lookups in the 50 m-resolution return map).

The model was validated by two methods: first, point comparisons with velocity time series in the main channel and from the intertidal study site; and second, for a more integrative measure, comparing tidal-excursion-scale horizontal diffusivity in the main channel with empirical values based on salinity time-series analysis (Banas et al., 2004). For the velocity validation, six velocity time-series stations were used, four in the main channel as described by Kraus (2000) and previously used for model validation by Banas and Hickey (2005), and two new intertidal stations, one towards shore (N46.59774°, W124.03021°) and one near the channel (N46.59790°, W124.02082°). Currents at these two intertidal stations were measured with acoustic Doppler current

profilers (Nortek Aquadopp) on 19 to 28 Jul 2008. Flow was determined for multiple 5 cm bins (north/south, east/west and up/down) beginning 10 cm off the bottom to within 10 cm of the surface of the water, and measurements were taken at 2 MHz at 10 minute intervals with a 0.05 m blanking distance. At both stations, water depth at mean high water was 2 m. Depth-averaged root mean square (rms) tidal velocity at all six stations from observations and the model are given in Table 1. Percent errors range from 1-35% with a mean of 15%, generally increasing up-estuary and shoreward, and generally in the direction of overestimated velocities and underestimated velocity gradients in the model. Note that this mode of error probably biases model results in a direction opposite to our conclusion that strong net-circulation gradients exist across intertidal flats.

For the horizontal diffusivity analysis, which measures the net, tidally averaged tidal circulation (as opposed to the amplitude of tidal currents themselves), we calculated diffusivities K_H at the five main-channel stations where observational estimates were previously reported (Banas et al., 2004), from the rate of horizontal dispersion of square patches of model particles the same width as the channel: $K_H = 1/2\ d\langle x^2\rangle/dt$, where t is time and $\langle x^2\rangle$ is the two-dimensional variance in particle positions around their center of mass. Like the Banas and Hickey (2005) model, this new version of the model replicates the high diffusivities (200-700 $m^2\ s^{-1}$) observed in moored salinity time series in the well-flushed outer 20 km of the estuary, where our study site is located.

In the poorly flushed, southern reaches of the bay, where observationally-derived horizontal diffusivities on the scale of the channel width are 50-100 $m^2\ s^{-1}$ (Banas and Hickey, 2005), the new ROMS model underestimates diffusivities by approximately a factor of two and predicts main-channel residence times ~25-50% higher than the Banas

and Hickey (2005) estimate. These discrepancies could result from both models' simple assumptions about bottom friction; bias in the depth of shallow tidal flats introduced in the merging of intertidal and subtidal bathymetric surveys; under-resolution of narrow, secondary and tertiary channels; or weak baroclinic effects. Since these issues do not seem to affect our study area and in any case would be difficult to pursue without extensive new observations, we have simply confined our analysis to the middle-to-outer estuary (Fig. 2), and refrain from speculating about residence time patterns across tidal flats in the southern bay.

2.3 Cross-shore pattern of temperature and salinity

Salinity can act as a passive tracer of water age, particularly when source water varies in salinity due, in this case, to coastal upwelling strength. We deployed multiparameter dataloggers (YSI Datasonde 6600) between 2 Jun and 28 Aug 2008 to record salinity (as specific conductivity), temperature, and water depth at five stations spanning 1 km from channel to shore (Fig. 3a, Table S1). Probes were suspended 0.1 m above the sediment, recording at 10-min intervals, and were cleaned every 2 wk. Sensors were held in a common water bath four times throughout the summer, and specific conductivity adjusted for two of the sensors showing consistent offsets from the others. Specific conductivity (mS/cm) was then converted to salinity (practical salinity units; Wagner et al., 2006). For the three-month period of deployment, median water levels were 1.6 m relative to MLLW. Seven measurements centered around the time of median water level were averaged on each flood tide at each sensor; this process standardized comparisons across the tidal flat.

The Bakun upwelling index for the time series point closest to Willapa Bay (48° N, 125° W) was used as an index of salinity in source water outside the bay (http://www.pfel.noaa.gov/products/PFEL/modeled/indices/upwelling/NA/data_download.html). For each of two sensors closest to the channel, each day's salinity (mean of two flood tides on most days) was related to the daily upwelling index using a linear model, and model fit (r^2, P value for n=63 or 68 days) was recorded for time lags of 0 to 7 days. Due to summer drought, these models also included day of year as a predictor to account for generally increasing salinity in the bay during the summer.

Two types of analyses were carried out to determine cross-shore gradients in temperature and salinity, testing each of three shoreward stations against the channel station with the most complete record (ChS). The first type emphasized mean differences in water properties based on paired t-tests (paired by each flood tide). The second type emphasized time lags in water properties by examining model fit (r^2 for n~75-130 flood tides) of the relationship between the times series at two sensors, with lags from the channel sensor of 0 to 4 tidal cycles.

2.4 Cross-shore pattern of chlorophyll concentration

Two approaches were taken to determine how chlorophyll concentration changed across the tidal flat, one involving fixed sensors and a second by motoring a sensor along transects from channel to shore. We deployed multiparameter dataloggers (YSI Datasonde 6600) between 2 and 15 Aug 2007 to record chlorophyll fluorescence, water depth, temperature, and salinity, at one near-channel station (ChN) and three towards shore (two of these three sensors were at ShMid; Fig. 3a, Table S1). Sensors spanned

0.56 km, with probes suspended 0.1 m above the sediment and recording at 10-min intervals. To make fluorescence readings consistent among sensors, the four sensors were held in common conditions while chlorophyll was altered by adding and filtering phytoplankton (14 levels), and adjustments were made to raw values so that all sensors had the same slope and zero intercept; however, no bottle samples were collected for calibration to chlorophyll-a, and so results are provided only as fluorescence. During field deployment, the sensors occasionally generated segments of particularly noisy data, in which both the values themselves and their change between 10-min intervals were large (i.e. corrected values >25 $\mu g\ L^{-1}$ and fluctuation >10 $\mu g\ L^{-1}$), possibly from catching drift macroalgae. We removed readings >25 $\mu g\ L^{-1}$ before proceeding to the next step of calculating tide-specific fluorescence. Seven measurements centered around the time of each median water level (1.6 m MLLW) were averaged for each flood and ebb tide for each sensor. We required at least three of the seven measurements to have passed the 25 $\mu g\ L^{-1}$ filter, and then removed any values >10 $\mu g\ L^{-1}$ from the mean fluorescence of other measurements. Also, strong drift in fluorescence was evident at one ShMid sensor for the last five days of deployment, and these means were included in visual display of all data but not used in analysis. Once these steps to generate means from reliable sections of fluorescence readings were complete, we calculated the difference in fluorescence (t-test, paired by tidal cycle) between each sensor and the one closest to the channel (ChN), separately for flood and ebb tides.

Chlorophyll concentrations were mapped across the tidal flat an hour before the afternoon high tide on 17 Aug 2008. This small boat-based sampling involved driving six transects from channel to shore while water was forced into the opening of a tube

under the boat, 0.2 m below the surface. The water then fed into a pipe holding a YSI Datasonde 6600, which measured temperature, salinity (as specific conductivity), and fluorescence every 5 seconds. A GPS (Garmin Geko) simultaneously recorded position. To calibrate the chlorophyll sensor, bottle samples were collected (300 ml in triplicate at three positions), extracted in 90% W/V acetone and frozen >24 h, and measured on a fluorometer (Turner Designs AU-10) following acidification procedure (Welschmeyer 1994). This calibration showed that the fluorescence values recorded by the sensor needed to be altered: Chlorophyll-a = 0.319 × Fluorescence (r^2=0.68, N=9). Each transect of about 0.5 km had 14-31 measurements at different distances from the channel (MLLW contour). Chlorophyll-a was considered a response variable and distance a predictor variable in linear models (regression) to calculate the slope and standard error for each transect. Then, meta-analysis procedures were applied to these six slopes and SE to calculate the overall change in chlorophyll with distance from the channel (rma command in package metafor; Viechtbauer, 2017).

2.5 Cross-shore pattern of oyster performance

Growth and condition of juvenile oysters (*Magallana = Crassostrea gigas*) were measured at five stations on the tidal flat where the overall bathymetry was sufficiently flat to enable deployment at a common tidal elevation, judged by water level (Fig. 3a). Distance to channel was determined for each station based on the MLLW contour, and ranged from 0.2 to 0.7 km (Table S1). Hatchery-raised oyster larvae were settled onto 11 x 11 cm unglazed ceramic tiles, thinned to 8-15 oysters per tile, and grown to a size of 1 cm shell length in a common location. On 3 Aug 2007, five tiles were attached vertically

to PVC poles at an elevation of +0.6 m MLLW at each of the five outplant stations. Tiles were always at least 0.15 m above the sediment, although this distance varied slightly among stations. Tiles were collected 19 May 2008, and all oysters were measured for maximum shell length from the umbo (shell height, mm). Subsequently, oyster meat was removed and dried (60°C, nearest 0.01 g) and a metric of condition developed as the ratio of dry meat weight to shell length. We were unable to remove bottom valves from the tiles, thus precluding the use of typical condition index based on ratios of tissue mass to internal shell volume (Lawrence and Scott, 1982). Of 25 tiles deployed, 23 were recovered. Of 171 oysters measured, three were removed from analysis because their tissue mass did not register on our balance (two from a shoreward station and one near the channel) and an additional one was censored because its weight was probably incorrectly recorded (order of magnitude more dry mass than any other oyster). Oyster shell height and condition were analyzed with linear mixed effects models, in which distance to channel was a fixed effect and tile was a random effect to account for multiple oysters per tile (package nlme, Pinheiro et al., 2016). Statistical significance was set at α=0.05. Analyses of water properties and oyster performance were performed in R (R Core Team, 2015). Empirical data underlying these analyses are archived at http://dx.doi.org/10.17632/wx9y9njnnr.1

3 Results

3.1 Water residence time

The ROMS numerical model showed a strong spatial pattern in intertidal residence time around our study site. Fig. 2 depicts the number of tidal cycles it takes for half of the 16 particles originating in each 200 x 200 m square in the intertidal zone to be found outside the intertidal zone at high water. This quantity is a proxy for the length of time that intertidal grazers have access to a particular water parcel. In our study region, this intertidal residence time varies from 0-4 tidal cycles over a distance of 2 km, with a reduced range over the 1-km tidal flat where stations for empirical measurements were located. Values are patchy, but generally increase toward shore. Gradients in residence time emerge on a number of wide tidal flats in the middle-to-outer estuary (Fig. 2), not only at our study site. However, the width of a particular tidal flat is not a reliable predictor of the mean or maximum intertidal residence time: examples can be found (Fig. 2) of narrow flats with residence time much greater than one cycle, and extensive intertidal flats where the outer portions are well-flushed within one cycle, as one might naively expect.

3.2 Cross-shore pattern of temperature and salinity

Upwelled, high-salinity water outside the bay reached the channel sensors after a 4-day lag (Fig. 4a, Table 2). The highest r^2 values were associated with 4-day lags, and model fit for salinity was significantly improved by including the Bakun upwelling index as a predictor, lagged by four days (likelihood ratio tests of models with no upwelling predictor vs. 4-day lag: ChN $F_{1,60}$=21.4, P<0.0001, ChS $F_{1,66}$=21.3, P<0.0001). Empirically, water properties at median flood tide differed between sensors deployed at channel and shore stations (Fig. 4b, c). Water at the station closest to shore (ChIn) was

0.58°C warmer than at the channel, and other shoreward stations followed this pattern (0.62°, 0.30°C warmer, Table 3). Salinity tended to be lower at shoreward stations relative to the channel stations and also lagged by one tidal cycle from channel to shore (Table 3). This lag is particularly evident in Fig. 4b for a portion of summer 2008 when salinity was initially lower towards shore and then reversed to be higher towards shore, as downwelled low-salinity water reached the shoreward portion of the tidal flat later than it appeared near the channel. No lags were necessary in the best fit model for the temperature time series, but a notable feature here was that lags of 0, 2, 4 tidal cycles fit better than lags of 1, 3 cycles (Table 3). This evidently arose due to the diurnal cycle in heating and cooling, with the warmer temperatures occurring during afternoon and early evening.

3.3 Cross-shore pattern of chlorophyll concentration

In general, fluorescence was low as water began to flood onto the tidal flat, then increased during the flood and declined during the ebb, especially at the channel station (Fig. 5c). On flood tides, the upstream station was near the channel and downstream stations towards shore. All downstream stations had significantly lower fluorescence than the channel station as water flooded through median water level (Fig. 5a, Table 4). During flood tides, the sensor at ShOut recorded 78% of the fluorescence relative to the channel station, and this proportion was even lower at the two ShMid sensors (37%, 64%). As the tide ebbed, the channel station was downstream from stations closer to shore, but still had greater or similar fluorescence relative to shoreward stations (Fig. 5b,

Table 4). Fluorescence did not differ at ShOut and ChN, but one of the ShMid sensors recorded lower fluorescence (47% relative to ChN).

Chlorophyll concentrations in surface water measured along transects also declined from channel to shore (Fig. 3b, Table S2). Chlorophyll-a at the start of each transect, closest to the channel, was 4.23 μg L^{-1}, and this declined at -2.99 μg L^{-1} km^{-1} (SE 0.53). Accordingly, over 0.5 km, the proportion of chlorophyll remaining was 65%.

3.4 Cross-shore pattern of oyster performance

Over nine months, juvenile oysters on tiles grew from about 1 cm to 3 cm. Final shell height of juvenile oysters did not differ with distance to channel ($t_{1,21}$=-0.27, p=0.8; Fig. 6a). However, condition (dry tissue weight per shell height) followed a channel-to-shore gradient (Fig. 6b). Condition declined 25% across the intertidal flat as oysters were 0.5 km further from the channel (Condition = 5.73 – 2.828 × Distance in km; $t_{1,21}$=-2.66, p=0.015). This pattern emerged even though tidal elevation and immersion time were held constant.

4 Discussion

The key result to emerge from both modeling and empirical work in our study is that heterogeneous water residence time on intertidal flats provides an additional mechanism for cross-shore physical and biological gradients, beyond the more obvious mechanisms of tidal elevation and upstream-downstream position, and despite water draining off the flat at each low tide. At the subtidal (tidally-averaged) scale, water found near shore at high tide tends to return to the intertidal zone every high water for a median of 4 tidal

cycles, whereas water near the channel is largely replaced every tidal cycle (Fig. 2). By examination of other tidal flats modeled in middle-to-outer Willapa Bay, it is clear that intertidal residence time is not a simple function of distance to channel or bathymetry; however, gradients in residence time only developed on wider (≥1 km) tidal flats, while heterogeneity appeared in model results at smaller scales (Fig. 2).

Residence-time gradients across tidal flats have two implications. First, food depletion must be thought of as a several-tidal-cycle process: although the water found on the tidal flat drains into the channel on every ebb tide, its return over several successive flood tides allows it to be repeatedly and intensively modified through interactions with the sediment and benthic organisms. Second, because of this process, tidal circulation may create gradients in food availability over an intertidal area of 1 km or less, because differences in water age allow neighboring water parcels to be subject to different levels of depletion even if grazing pressure is spatially uniform.

Do such multi-day water residence times, as predicted by the numerical model reported here, as well as a prior iteration (Banas et al., 2007), actually occur on intertidal flats? Observations of physical (salinity) and biological (chlorophyll) water properties indicate that they do. Weather-event-scale fluctuations in salinity show a time lag (one tidal cycle) from channel to shore, indicating that the water towards shore takes longer to be replaced than water near the channel: the tidal flat is not renewed as a single unit on each flood tide. Note that the lag of 1 tidal cycle was measured over a smaller distance than the full tidal flat width over which the model predicts a residence time gradient from 0–4 cycles, and also that the lag time is a different physical quantity (signal

propagation time through an oscillatory boundary layer: Batchelor, 1967) from a residence time estimate.

For chlorophyll, it is necessary to ask whether the observed gradients could have been achieved through suspension-feeding as the water transited between sensors during a single flood tide (as in Fig. 1a), or whether a longer period of interaction is required (Fig. 1b). Key parameters to distinguish these processes are available from prior studies of this tidal flat in which parcels of water were tracked with Lagrangian drifters (Wheat and Ruesink, 2013): exponential loss rates of chlorophyll were -0.24 h^{-1} due to the feeding of benthic suspension-feeders, while water velocity averaged 0.16 m s^{-1}, consistent with model results and stationary sampling (Table 1). The loss rate of -0.24 h^{-1} was measured at water depths <1.2 m (Wheat and Ruesink, 2013), and so represents an upper bound (i.e. rapid decline) in which suspension feeders affect a small volume of overlying water. Recall that ShMid sensors showed 37% and 64% of fluorescence relative to ChN, and these sensors were separated by 0.56 km east-west (1 h at 0.16 m s^{-1}), giving loss rates of -0.99 and -0.44 h^{-1}. Thus the observed decline was two to four times greater than could be explained by a single passage of water between the stations. Additionally, during ebb tides, stations near the channel were in a downstream position relative to suspension-feeding occurring on the tidal flat. However, compression, rather than reversal, of the channel-to-shore gradient occurred on ebb relative to flood tides (Fig. 4). That is, on ebb tides, the shoreward stations were still lower in fluorescence than expected from a simple consideration of water influenced during a single transit between stations.

Transects from channel to shore showed that chlorophyll declined to 65% over 0.5 km (0.87 h at 0.16 m s^{-1}; Fig. 3b, Table S2), a loss rate of -0.50 h^{-1}. As such, empirical data from transects concurred with fixed sensors in demonstrating greater chlorophyll losses in water towards shore than expected from suspension-feeding in even-aged water. The results were consistent despite different methods, e.g., measurements on transects within 0.2 m of the water surface, but within 0.1 m of the sediment for fixed sensors. Fixed sensors gave further insight into mechanisms underlying gradients in chlorophyll concentrations through examination of the time series at 10-min resolution. Specifically, the first water to flood onto the tidal flat and reach the stations near the channel was low in fluorescence (Fig. 5c), suggesting older, depleted water that mixed only weakly with newer, chlorophyll-rich water while in the channel during low slack tide (cf. MacDonald, 2006).

Our conclusion that cross-shore gradients in chlorophyll were established through multiple passes of water over the tidal flat needs to be evaluated in light of several other factors known to limit draw-down by suspension feeders. Growth dynamics of phytoplankton (Calbet and Landry, 2004) and/or resuspension from the benthos (Ruesink et al., 2019) would tend to make our loss rates underestimates. Effects of suspension feeders on chlorophyll are also expected to be diluted as water depth increases. Overall, each of these factors would make residence-time variation less important to cross-shore gradients in chlorophyll, yet we nevertheless found empirical gradients greater than could be explained by benthic suspension-feeding during a single transit of water.

In contrast to salinity and chlorophyll, which supported that water appeared multiple times on the tidal flat, temperature was modified primarily within tidal cycles. We draw this conclusion due to the absence of statistical lags between channel and shoreward stations (Table 3), but also from strong diel variability in temperature. Water temperatures were warmer during daytime than nighttime flood tides, and also exhibited stronger channel-to-shore gradients during the day (Fig. 4c). Indeed, the first water to reach the shoreward sensor as the tide flooded in late afternoon was overall highest in temperature (Fig. 5d), as its small volume was heated by contact with dark sediment. In aggregate, these observations are consistent with water being heated as it travels over solar-heated sediment and cooled at night, making residence time effects less apparent. The distinction may arise because salinity is a conservative tracer and chlorophyll is likely to accumulate benthic influence in one direction only, whereas water temperatures may be modified in both positive and negative directions by a variety of heat-budget drivers acting at shorter time scales than residence time.

Food limitation due to draw-down of water column resources by other suspension feeders has been documented at two scales: at a scale of near neighbors, for instance in shellfish aquaculture stocked at high densities (Newell, 1990; Muschenheim and Newell, 1992; Senechal et al., 2008; Grangere et al., 2010), and at whole-basin scales when feeding by suspension feeders exceeds the delivery or growth of phytoplankton (Alpine and Cloern, 1992). In some cases, delivery of water column resources is not tightly linked to benthic secondary production, where the diet of suspension-feeders is dominated by resuspended microphytobenthos (Kang et al., 2003; Herman et al., 2000; van Oevelen et al., 2006). Nevertheless, competition impacts not

only near neighbors, by creating local regions of food depletion (Lenihan, 1999; Grangere et al., 2010), but also the food availability for distant individuals when extended water residence time allows for significant filtration. Secondary productivity on the tidal flat is accordingly driven by a complex interaction between filtration and residence time dynamics. Other studies have found similarly complex relationships between plankton dynamics, water advection and benthic secondary productivity (Tweddle et al., 2005; Simpson et al., 2007). Despite these complexities, the connection between (low) residence time and (high) bivalve carrying capacity has long been known at whole-estuary scales (Dame and Prins, 1998; Zu Ermgassen et al., 2013). Lower oyster condition is therefore consistent with longer water residence time towards shore, controlling for tidal elevation. Although shell growth did not follow a cross-shore gradient (Fig. 6), condition is the primary economic benchmark on this tidal flat, which is a fattening ground for oysters (Hedgpeth and Obrebski, 1981).

As expected in an estuary, salinity generally increased with water level as oceanic water was advected into the estuary on each flood tide (Fig. 5d). This is consistent with earlier conclusions (Roegner et al., 2002; Banas et al., 2007) that in this coastal-upwelling-driven system, phytoplankton are primarily supplied by the coastal ocean and progressively depleted within the estuary, such that high chlorophyll is correlated with high salinity, both across the tidal flat and across the tidal cycle within stations (Fig. 5c,d, Table S2).

Estuaries are typically described as heterogeneous in their along-axis dimension, including both physical and biological gradients (Attrill and Rundle, 2002; Ruesink et al., 2015; Tweedley et al., 2016). Orthogonal to this axis, as depth is reduced and flats

emerge at low tide, water flow and residence time can be influenced by wind, small bathymetric features such as hummocks and sloughs, and seawater-porewater exchange (Pokavanich and Alosairi, 2014; Sullivan et al., 2015). To our knowledge, no prior reports exist (other than Banas et al., 2007) of heterogeneity in multi-day residence time on intertidal flats, although extended residence times towards shore can be inferred from general principles if water reaching shallower depths is restricted in mixing with new ocean water (Hsu et al., 2013). Our empirical measurements of water properties support the existence of residence time variation at scales of 0.5-1 km intertidally, which effectively lengthens the time scale over which upstream suspension-feeders may modify resource delivery underlying benthic secondary production. The sedimentary characteristics of tidal flats are now understood as a predictable function of sediment supply and ratio of tidal currents to waves (Gao, 2019); however, water properties across these flats require further scrutiny to determine which morphological and hydrodynamic factors may lead to multi-day residence times.

Acknowledgements

This work was funded in part by a grant from Washington Sea Grant, University of Washington, pursuant to National Oceanic and Atmospheric Administration Award No. NA07OAR4170007. The views expressed herein are those of the authors and do not necessarily reflect the views of NOAA or any of its sub-agencies. We appreciate help from S. Yang, A. Norman, A. Trimble, M. Logsdon, K. Bennett, and T. Alcock. B. Dumbauld and L. McCoy provided the aerial photograph. Site access and insight came from K. and F. Wiegardt of Jolly Roger Oysters.

References

Abelson, A., Denny, M., 1997. Settlement of marine organisms in flow. Ann. Rev. Ecol. Syst. 28, 317-339.

Alpine, A.E., Cloern, J.E., 1992. Trophic interactions and direct physical effects control phytoplankton biomass and production in an estuary. Limnol. Oceanogr. 37, 946–955.

Attrill, M.J., Rundle, S.D., 2002. Ecotone or ecocline: Ecological boundaries in estuaries. Est. Coastal Shelf Sci. 55, 929-936.

Banas, N.S., Hickey, B.M., 2005. Mapping exchange and residence time in a model of Willapa Bay, Washington, a branching, macrotidal estuary. J. Geophysical Res.-Oceans 110(C11), 10.1029/2005JC002950.

Banas, N.S., Hickey, B.M., MacCready, P., Newton, J.A., 2004. Dynamics of Willapa Bay, Washington: A highly unsteady, partially mixed estuary. J. Phys. Oceanogr. 34, 2413–2427.

Banas, N.S., Hickey, B.M., Newton, J.A., Ruesink, J.L., 2007. Tidal exchange, bivalve grazing, and patterns of primary production in Willapa Bay, Washington, USA. Mar. Ecol. Prog. Ser. 341, 123–139.

Banas, N.S., MacDonald, P.S., Armstrong, D.A., 2009. Green crab larval retention in Willapa Bay, Washington: An intensive Lagrangian modeling approach. Est. Coasts 32, 893-905.

Batchelor, G.K., 1967: An Introduction to Fluid Dynamics. Cambridge University Press, 615 pp.

Bishop, M.J., Peterson, C.H., 2006. Direct effects of physical stress can be counteracted by indirect benefits: oyster growth on a tidal elevation gradient. Oecologia 147, 426-433.

Brown, J.R., Hartwick, E.B., 1988. Influences of temperature, salinity and available food upon suspended culture of the Pacific oyster, *Crassostrea gigas*: I. absolute and allometric growth. Aquaculture 70, 231–251.

Calbet, A., Landry, M.R., 2004. Phytoplankton growth, microzooplankton grazing, and carbon cycling in marine systems. Limnol. Oceanogr. 49, 51-57.

Dame, R., Prins, T.C., 1998. Bivalve carrying capacity in coastal ecosystems. Aquatic Ecol. 31, 409–421.

Dettmann, E.H., 2001. Effect of water residence time on annual export and denitrification of nitrogen in estuaries: A model analysis. Estuaries 24, 481–490.

Dittman, S., 2000. Zonation of benthic communities in a tropical tidal flat of north-east Australia. J. Sea Res. 43, 33-51.

Dumbauld, B.R., McCoy, L.M., 2015. Effect of oyster aquaculture on seagrass *Zostera marina* at the estuarine landscape scale in Willapa Bay, Washington (USA). Aquaculture Environment Interactions 7, 29-47.

Feldman, K.L., Armstrong, D.A., Dumbauld, B.R., DeWitt, T.H., Doty, D.C., 2000. Oysters, crabs, and burrowing shrimp: Review of an environmental conflict over aquatic resources and pesticide use in Washington State's (USA) coastal estuaries. Estuaries 23, 141–176.

Gangnery, A., Chabirand, J.M., Lagarde, F., Le Gall, P., Oheix, J., Bacher, C., Buestel, D., 2003. Growth model of the Pacific oyster, *Crassostrea gigas*, cultured in Thau Lagoon (Mediterranee, France). Aquaculture 215, 267–290.

Gao, S. 2019., Geomorphology and sedimentology of tidal flats. Pp 359-381 in (Perillo, G.M.E., Wolanski, E., Cahoon, D.R., Hopkinson, C.S., eds) Coastal Wetlands: an integrated ecosystem approach, 2nd ed. Elsevier.

Grangeré, K., Lefebvre, S., Bacher, C., Cugier, P., Ménesguen, A., 2010. Modelling the spatial heterogeneity of ecological processes in an intertidal estuarine bay: dynamic interactions between bivalves and phytoplankton. Mar. Ecol. Prog. Ser. 415, 141-158.

Grizzle, R., Greene, J., Coen, L., 2008. Seston removal by natural and constructed intertidal Eastern oyster (*Crassostrea virginica*) reefs: A comparison with previous laboratory studies, and the value of in situ methods. Est. Coasts 31, 1208–1220.

Harrison, S.J., Phizacklea, A.P., 1987. Temperature fluctuation in muddy intertidal sediments, Forth Estuary, Scotland. Est. Coastal Shelf Sci. 24, 279-288.

Hedgpeth, J.W., Obrebski, S., 1981. Willapa bay: a historical perspective and a rationale for research. Office of Biological Services, US Fish and Wildlife Service, Washington, D.C. FWS/OBS-81/03. 52 pp.

Herman, P.M.J., Middleburg, J.J., Widdows, J., Lucas, C.H., Heip, C.H.R., 2000. Stable isotopes as trophic tracers: combining field sampling and manipulative labeling of food resources for macrobenthos. Mar. Ecol. Prog. Ser. 204, 79-92.

Hickey, B.M., Banas, N.S., 2003. Oceanography of the U.S. Pacific Northwest coast and estuaries with application to coastal ecology. Estuaries 26, 1010-1031.

Hickey, B.M., Zhang, X., Banas, N., 2002. Coupling between the California Current System and a coastal plain estuary in low riverflow conditions. J. Geophys. Res. 107(C10), 1029/1999JC000160.

Hsu, K., Stacey, M.T., Holleman, R.C., 2013. Exchange between an estuary and an intertidal marsh and slough. Est. Coasts 36, 1137-1149.

Kang, C.K., Kim, J.B., Lee, K.S., Kim, J.B., Lee, P.Y., Hong, J.S., 2003. Trophic importance of benthic microalgae to macrozoobenthos in coastal bay systems in Korea: dual stable C and N isotope analyses. Mar. Ecol. Prog. Ser. 259, 79-92.

Kraus, N.C., 2000. Study of navigation channel feasibility, Willapa Bay, Washington. Final Report. US Army Corps of Engineers Seattle District, Seattle. ERDC/CHL TR, 00-06.

Lawrence, D.R., Scott, G.I., 1982. The determination and use of condition index in oysters. Estuaries 5, 23-27.

Lenihan. H.S., 1999. Physical-biological coupling on oyster reefs: How habitat structure influences individual performance. Ecol. Monogr. 69, 251– 275.

Lenihan, H.S., Peterson, C.H., Allen, J.M., 1996. Does flow speed also have a direct effect on growth of active suspension-feeders: An experimental test on oysters. Limnol. Oceanogr. 41, 1359–1366.

Lomovasky, B.J., Brey, T., Kluegel, A., Iribarne, O., 2018. Distribution pattern, density and growth of the stout razor clam *Tagelus plebeius* in a South-west Atlantic estuarine system. J. Mar. Biol. Assoc. UK 98, 485-494.

MacDonald, D.G., 2006. Estimating an estuarine mixing and exchange ratio from boundary data with application to Mt. Hope Bay (Massachusetts/Rhode Island). Est. Coastal Shelf Sci. 70, 326-332.

Muschenheim, D.K., Newell, C.R.,1992. Utilization of seston flux over a mussel bed. Mar. Ecol. Prog. Ser. 85, 131-136.

Newell, C.R., 1990. Effects of mussel (*Mytilus edulis*, Linnaeus, 1758) position in seeded bottom patches on growth at subtidal lease sites in Maine. J. Shellfish Res. 9, 113-118.

Oey, L.Y., 2005. A wetting and drying scheme for POM. Ocean Modelling 9, 133-150.

Peterson, C.H., 1991. Intertidal zonation of marine invertebrates in sand and mud. American Scientist 79, 236-249

Peterson. C.H., Black, R., 1987. Resource depletion by active suspension feeders on tidal flats -influence of local density and tidal elevation. Limnol. Oceanogr. 32, 143–166.

Pinheiro, J., Bates, D., DebRoy, S., Sarkar, D., R Core Team., 2016. nlme: Linear and Nonlinear Mixed Effects Models. R package version 3.1-128, http://CRAN.R-project.org/package=nlme.

Pokavanich, T., Alosairi, Y., 2014. Summer flushing characteristics of Kuwait Bay. J. Coastal Res. 30, 1066-1073.

R Core Team, 2015. R: A Language and Environment for Statistical Computing. R Foundation for Statistical Computing, Vienna, Austria.

Ren, J.S., Ross, A.H., 2001. A dynamic energy budget model of the Pacific oyster *Crassostrea gigas*. Ecol. Modelling 142, 105-120.

Roegner, G.C., Hickey, B.M., Newton, J.A., Shanks, A.L., Armstrong, D.A., 2002. Wind-induced plume and bloom intrusions into Willapa Bay, Washington. Limnol. Oceanogr. 47, 1033–1042.

Ruesink, J.L., Roegner, G.C., Dumbauld, B.R., Newton, J.A., Armstrong, D.A., 2003. Contributions of coastal and watershed energy sources to secondary production in a northeastern pacific estuary. Estuaries 26, 1079–1093.

Ruesink, J.L., Yang, S., Trimble, A.C., 2015. Variability in carbon availability and eelgrass (*Zostera marina*) biometrics along an estuarine gradient in Willapa Bay, Washington, USA. Est. Coasts 38, 1908-1917.

Ruesink, J.L., Donoghue, C.R., Horwith, M.J., Lowe, A.T., Trimble, A.C., 2019. Comparison of shallow-water seston among biogenic habitats on tidal flats. PeerJ 7, e6616, https://doi.org/10.7717/peerj.6616.

Ruiz, C., Abad, M., Sedano, F., Garcia-Martin, L.O., Sanchez Lopez, J.L., 1992. Influence of seasonal environmental changes on the gamete production and biochemical composition of *Crassostrea gigas* (Thunberg) in suspended culture in El Grove, Galicia, Spain. J. Exp. Mar. Biol. Ecol. 155, 249–262.

Ryu, J., Khim, J.S., Choi, J.W., Shin, H.C., An, S., Park, J., Kang, D., Lee, C.H., Koh, C.H., 2011. Environmentally associated spatial changes of a macrozoobenthic community in the Saemangeum tidal flat, Korea. J. Sea Res. 65, 390-400.

Senechal, J., Grant, J., Archambault, M.C., 2008. Experimental manipulation of suspended culture socks: Growth and behavior of juvenile mussels (*Mytilus* spp.). J. Shellfish Res. 27, 811–826.

673 Simpson, J.H., Berx, B., Saurel, C., 2007. The interaction of tidal advection, diffusion
674 and mussel filtration in a tidal channel. J. Mar. Systems 68, 556–568.
675 Sullivan, J.C., Torres, R., Garrett, A., Blanton, J., Alexander, C., Robinson, M., Moore,
676 T., Amft, J., Hayes, D., 2015. Complexity in salt march circulation for a
677 semienclosed basin. J. Geophys. Res.-Earth Surface 120, 1973-1989.
678 Tomiyama, T., Komizunai, N., Ito, K., Omori, M., 2010. Spatial variation in the
679 abundance and condition of the bivalve *Nuttallia olivacea* in relation to
680 environmental factors and sublethal predation. Mar. Ecol. Prog. Ser. 406, 185-196.
681 Tweddle, J.F., Simpson, J.H., Janzen, C.D., 2005. Physical controls of food supply to
682 benthic filter feeders in the Menai Strait. Mar. Ecol. Prog. Ser. 289, 79-88.
683 Tweedley, J.R., Warwick, R.M., Potter, I.C., 2016. The contrasting ecology of temperate
684 macrotidal and microtidal estuaries. Oceanogr. Mar. Biol. Ann. Rev. 54, 73-171.
685 van Oevelen, D., Soetart, K., Middelburg, J.J., Herman, P.M.J., Moodley, L., Hamels, I.,
686 Moens, T., Heip, C.H.R., 2006. Carbon flows through a benthic food web:
687 Integrating biomass, isotope and tracer data. J. Mar. Res. 64, 453-482.
688 Viechtbauer, W., 2017. Package ‘metafor’. http://www.metafor-project.org
689 Wagner, R.J., Boulger, R.W. Jr., Oblinger, C.J., Smith, B.A., 2006. Guidelines and
690 standard procedures for continuous water-quality monitors—Station operation,
691 record computation, and data reporting: U.S. Geological Survey Techniques and
692 Methods 1–D3, 51 pp., http://pubs.water.usgs.gov/tm1d3.
693 Walles, B., Smaal, A.C., Herman, P.M.J., Ysebaert, T., 2016. Niche dimension differs
694 among life-history stages of Pacific oysters in intertidal environments. Mar. Ecol.
695 Prog. Ser. 562, 113-122.

Warner, J.C., 2010. Using a composite grid approach in a complex coastal domain to estimate estuarine residence time. Computers and Geosciences 36, 921–935.

Welschmeyer, N.A., 1994. Fluorometric analysis of Chlorophyll-a in the presence of Chlorophyll-b and pheopigments. Limnol. Oceanogr. 39, 1985–1992.

Wheat, E.E., Ruesink, J.L., 2013. Commercially-cultured oysters (*Crassostrea gigas*) exert top-down control on intertidal pelagic resources in Willapa Bay, Washington, USA. J. Sea Res. 81, 33-39.

Wiberg, P.L., Carr, J.A., Safak, I., Anutaliya, A., 2015. Quantifying the distribution and influence of non-uniform bed properties in shallow coastal bays. Limnol. Oceanogr.-Methods 13, 746-762.

Whyte, J.N.C., Englar, J.R., Carswell, B.L., 1990. Biochemical composition and energy reserves in *Crassostrea gigas* exposed to different levels of nutrition. Aquaculture 90, 157–172.

Xue, H., Du, Y., 2010. Implementation of a wetting-and-drying model in simulating the Kennebec Androscoggin plume and the circulation in Casco Bay. Ocean Dynamics 60, 341–357.

Zu Ermgassen, P.S.E., Gray, M.W., Langdon, C.J., Spalding, M.D., Brumbaugh, R.D., 2013. Quantifying the historic contribution of Olympia oysters to filtration in Pacific Coast (USA) estuaries: implications for restoration objectives. Aquatic Ecol. 47, 149-161.

FIGURE LEGENDS

Figure 1. Two mechanisms for the depletion of phytoplankton from a parcel of water by intertidal suspension-feeders. In the familiar case (a), the parcel is depleted during its passage across the intertidal zone on a single flood tide. In the case discussed in this paper (b), the parcel is depleted over several successive passages across the intertidal zone, returning due incomplete mixing in the channel at low slack tide. Parcels of water can be considered to have a residence time exceeding one tidal cycle. The length of time available for suspension-feeders to influence a parcel of water is controlled by the tidally averaged residual circulation (dotted arrow), rather than the tidal currents themselves.

Figure 2. Water residence time on intertidal flats in Willapa Bay, Washington, from particle-tracking analysis of a 50 m-resolution numerical model with realistic intertidal bathymetry. Residence time (color scale, in units of tidal cycles) is the length of time that more than half of the 16 particles released in each 200 m square at high tide continue to be found in the intertidal zone at successive high tides, despite draining into the deeper channels in between. Solid contours give subtidal bathymetry at 5 m intervals. Box surrounds study site, as depicted in Fig. 3.

Figure 3. Tidal flat in Willapa Bay. The same area is depicted in (a) and (b), also corresponding to the boxed area in Fig. 2. (a) Aerial photograph overlaid with five stations where water properties and oyster performance were measured: South channel (ChS), North channel (ChN), Outer shore (ShOut), Middle shore (ShMid), and Inner shore (ShIn). Sensors were placed in 2007 for chlorophyll measurements (Chl) and in

2008 for measurements of temperature and salinity (TS). Oysters were outplanted on tiles for 10 months. (b) Chlorophyll-a (μg L^{-1}) along six transects one hour prior to afternoon high tide on 17 Aug 2008. The sensor recorded no data during three 50-sec periods, evident as gaps in transects.

Figure 4. Temperature and salinity at the median water level on flood tides across a tidal flat in Willapa Bay. (a) Salinity at near-channel stations linked to upwelling at 48°N 125°W. Upwelling is plotted with a 4-day lag, which represents the best correlation (Table 2). Salinity is a daily average of two flood tides. The portion of this summer-long time series from 4 to 15 August is shown in more detail, distinguishing each flood tide, in subsequent panels. (b) Salinity and (c) water temperature at a near-channel station and three stations toward shore. Station codes are in Fig. 3.

Figure 5. Water column fluorescence at four stations across a tidal flat in Willapa Bay on each a) flood and b) ebb tide in 2007. Open symbols show values from one ShMid station where the sensor demonstrated strong drift during the last five days of deployment, and these values were not used in analyses. The following two panels show (c) fluorescence and (d) water temperature and salinity for six tidal cycles of data logged at 10-min intervals at one channel and one shore sensor during the early portion of the time series (2 Aug to 6 Aug 2007). Because fluorescence values exceeding 25 μg L^{-1} were censored, the data series is interrupted for ChN after the fourth tidal cycle, and no values were calculated around median water level. Station codes are in Fig. 3.

Figure 6. Performance of Pacific oysters (*Magallana* = *Crassostrea gigas*) across a tidal flat in Willapa Bay. A) Shell height, B) Condition, as dry flesh mass relative to shell height. Open points are individual oysters; dark points show means per tile. Oysters were outplanted at 1 cm in Aug 2007 and collected in May 2008. X-axis is reversed so that shore is to left and channel to right, to align with Fig. 2 and 3. Station codes are defined in Fig. 3.

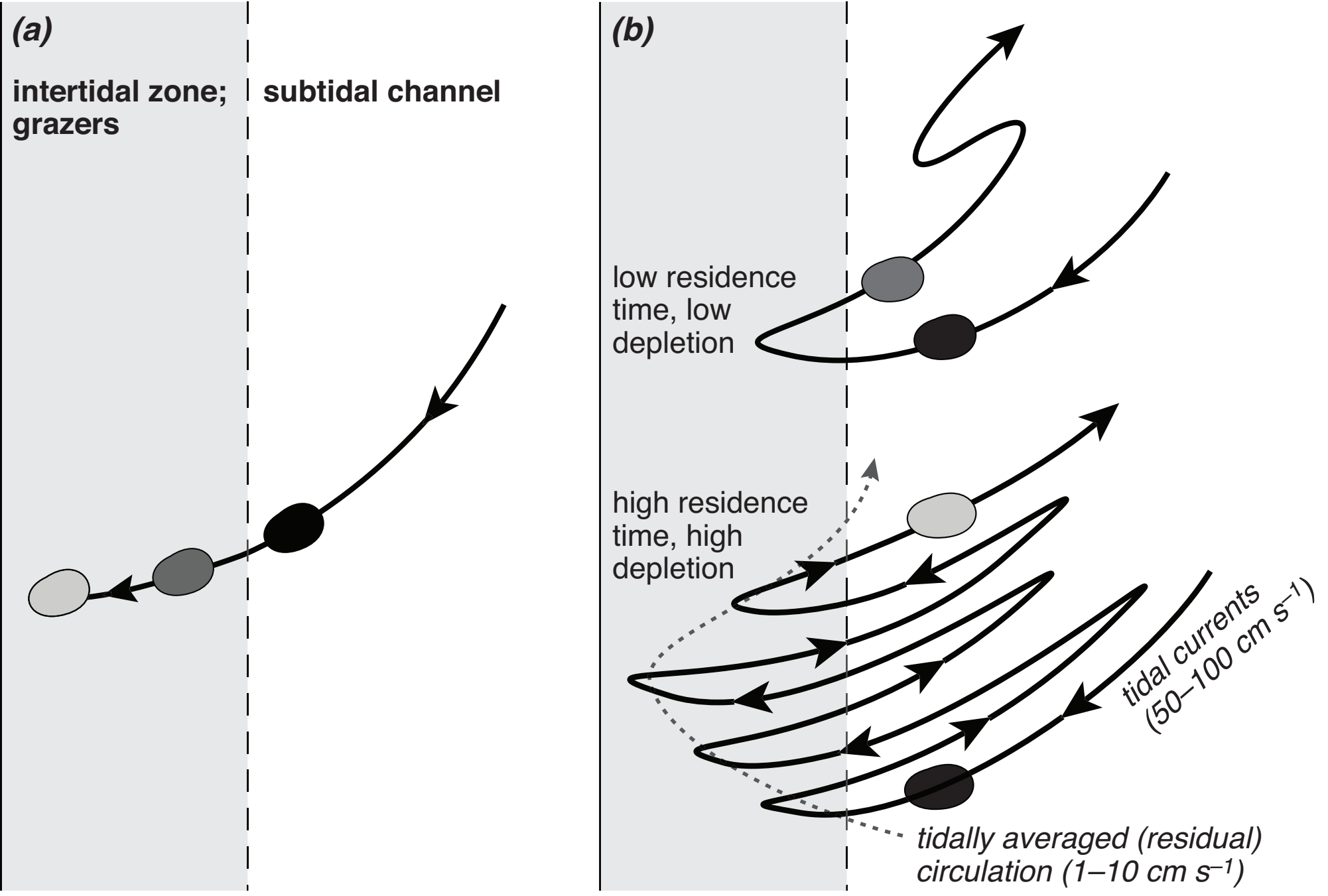
(a)
intertidal zone; grazers
subtidal channel
(b)
low residence time, low depletion
high residence time, high depletion
tidal currents (50–100 cm s–1)
tidally averaged (residual) circulation (1–10 cm s–1)

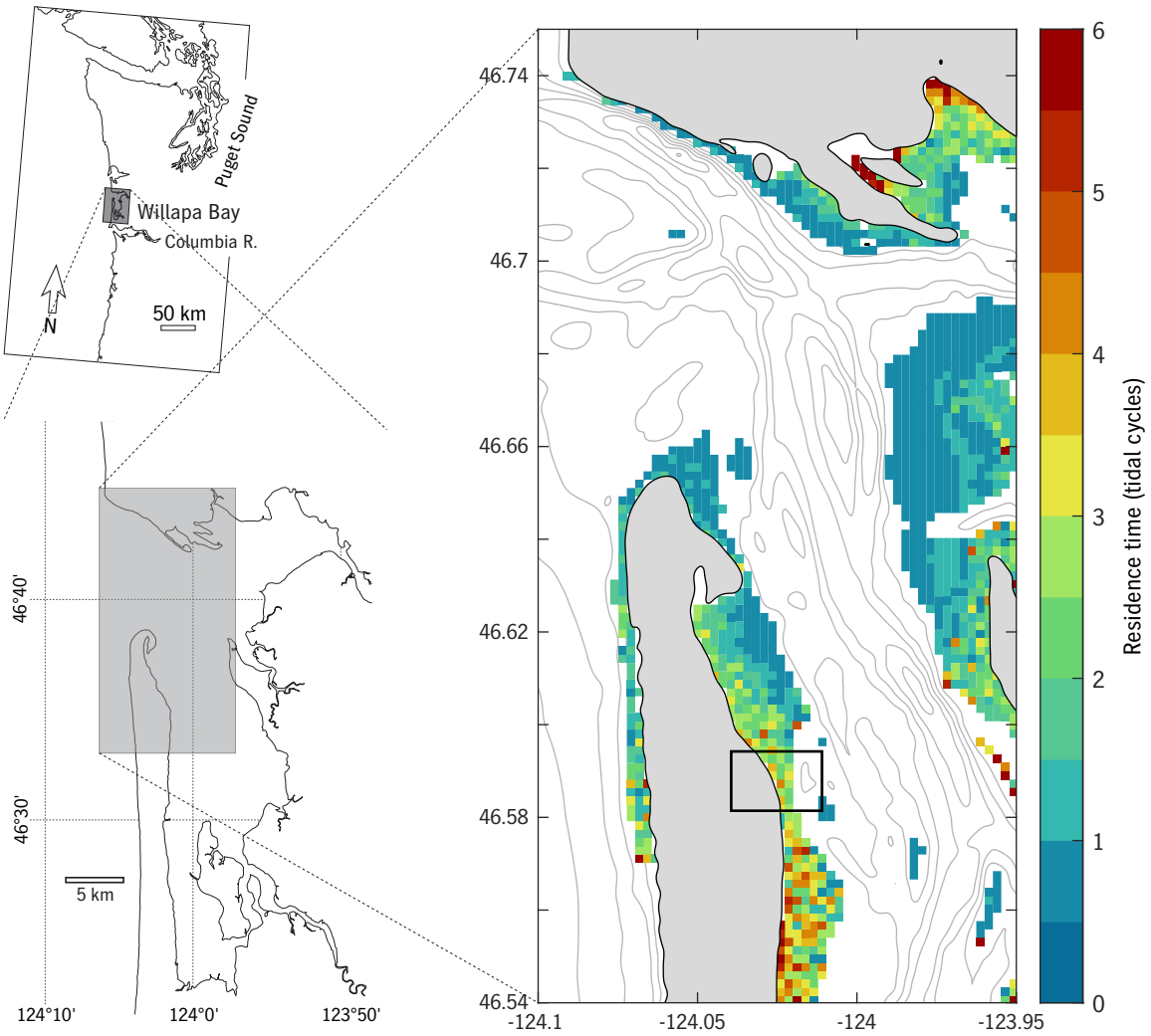
Puget Sound
Willapa Bay
Columbia R.
N
50 km
5 km
46°40'
46°30'
124°10'
124°0'
123°50'
46.74
46.7
46.66
46.62
46.58
46.54
-124.1
-124.05
-124
-123.95
Residence time (tidal cycles)
0
1
2
3
4
5
6

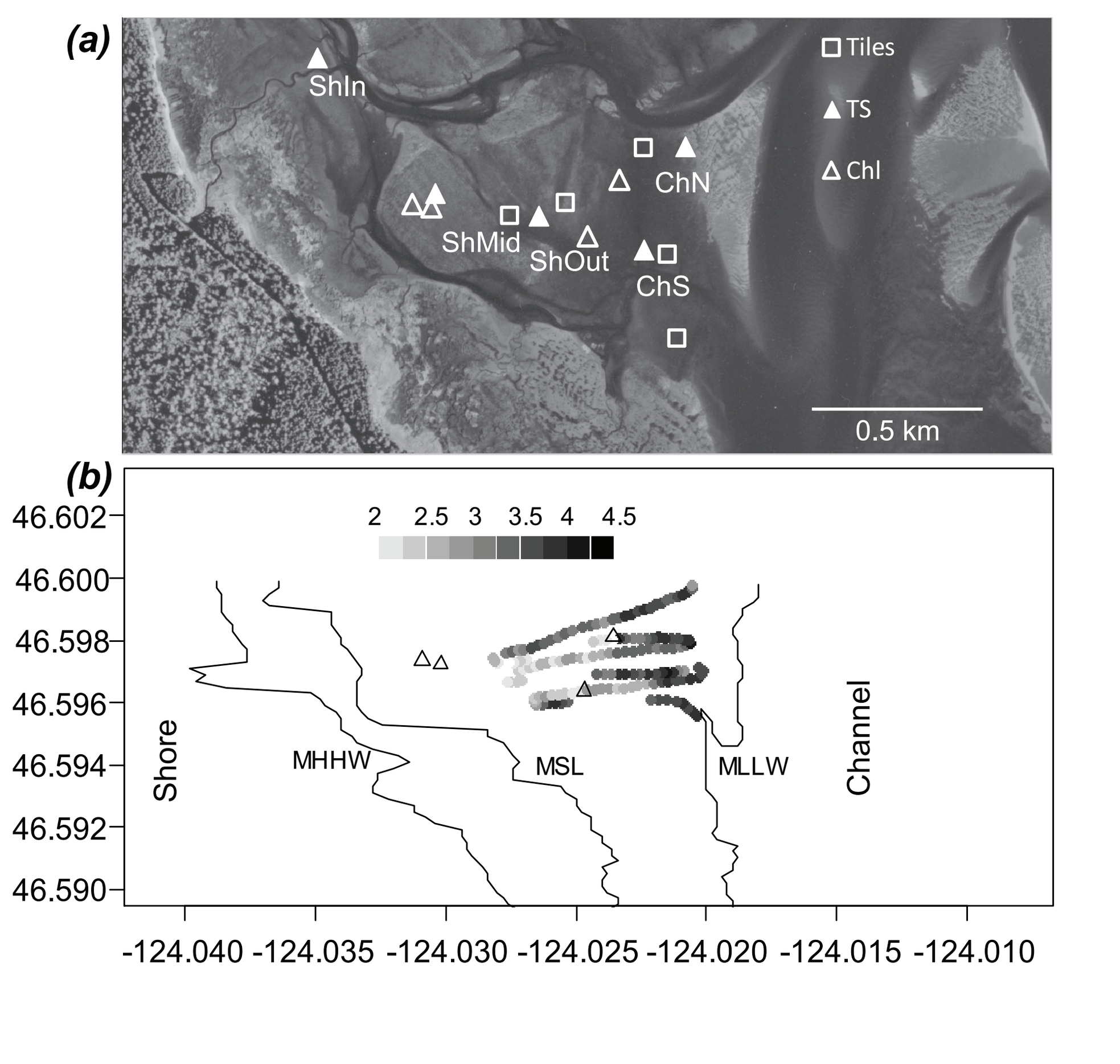
(a)
ShIn
ShMid
ShOut
ChN
ChS
Tiles
TS
Chl
0.5 km
(b)
2 2.5 3 3.5 4 4.5
46.602
46.600
46.598
46.596
46.594
46.592
46.590
Shore
MHHW
MSL
MLLW
Channel
-124.040 -124.035 -124.030 -124.025 -124.020 -124.015 -124.010

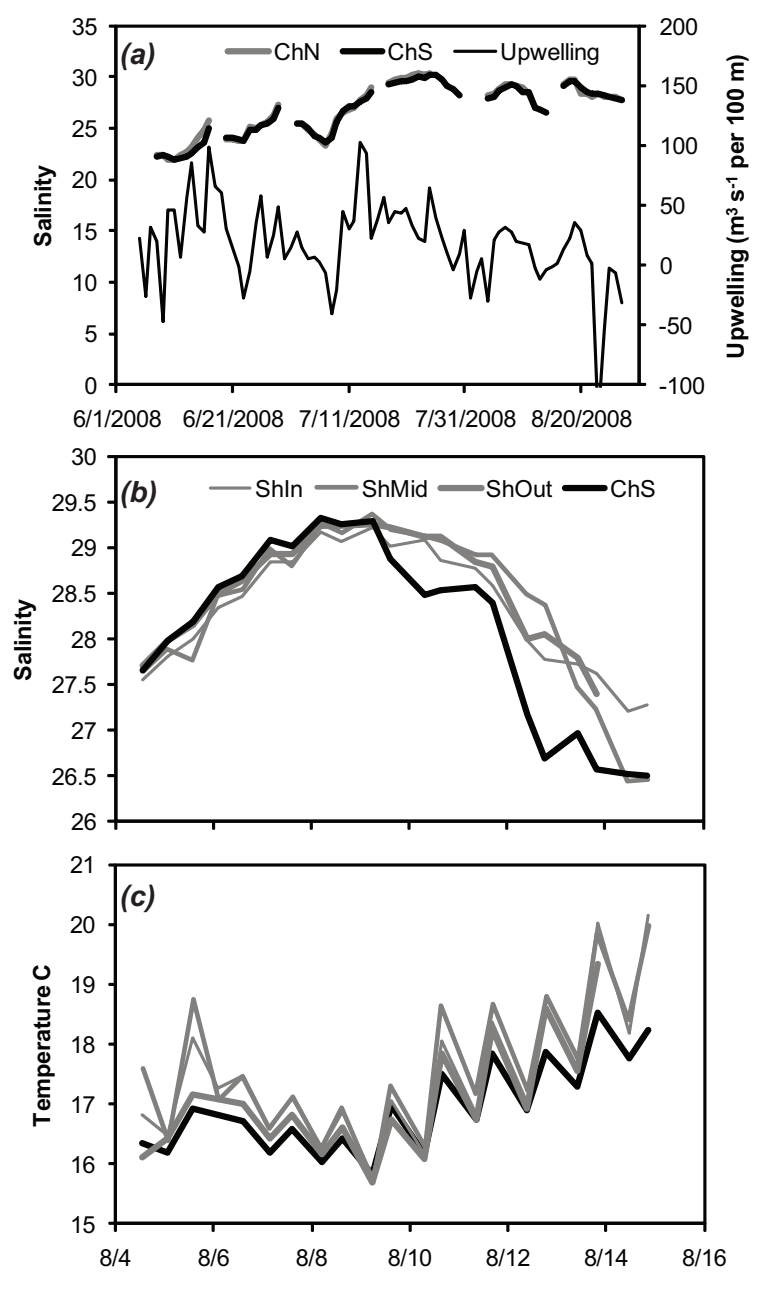
(a)
ChN
ChS
Upwelling
Salinity
Upwelling (m³ s⁻¹ per 100 m)
35
30
25
20
15
10
5
0
200
150
100
50
0
-50
-100
6/1/2008
6/21/2008
7/11/2008
7/31/2008
8/20/2008
(b)
ShIn
ShMid
ShOut
ChS
Salinity
30
29.5
29
28.5
28
27.5
27
26.5
26
(c)
Temperature C
21
20
19
18
17
16
15
8/4
8/6
8/8
8/10
8/12
8/14
8/16

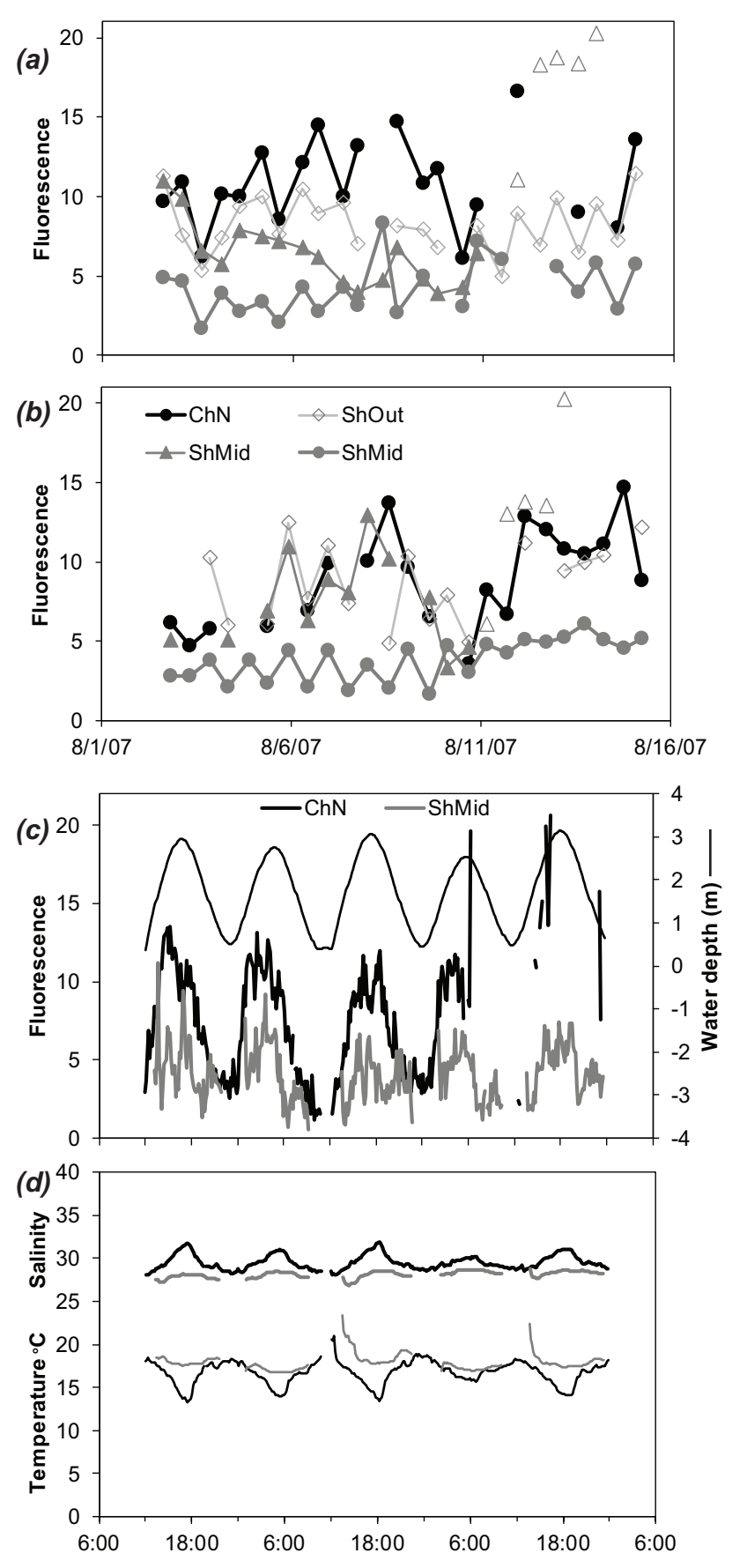
(a)
Fluorescence
20
15
10
5
0
(b)
ChN
ShOut
ShMid
ShMid
Fluorescence
20
15
10
5
0
8/1/07
8/6/07
8/11/07
8/16/07
(c)
ChN
ShMid
Fluorescence
Water depth (m)
20
15
10
5
0
4
3
2
1
0
-1
-2
-3
-4
(d)
Salinity
Temperature °C
40
35
30
25
20
15
10
5
0
6:00
18:00
6:00
18:00
6:00
18:00
6:00

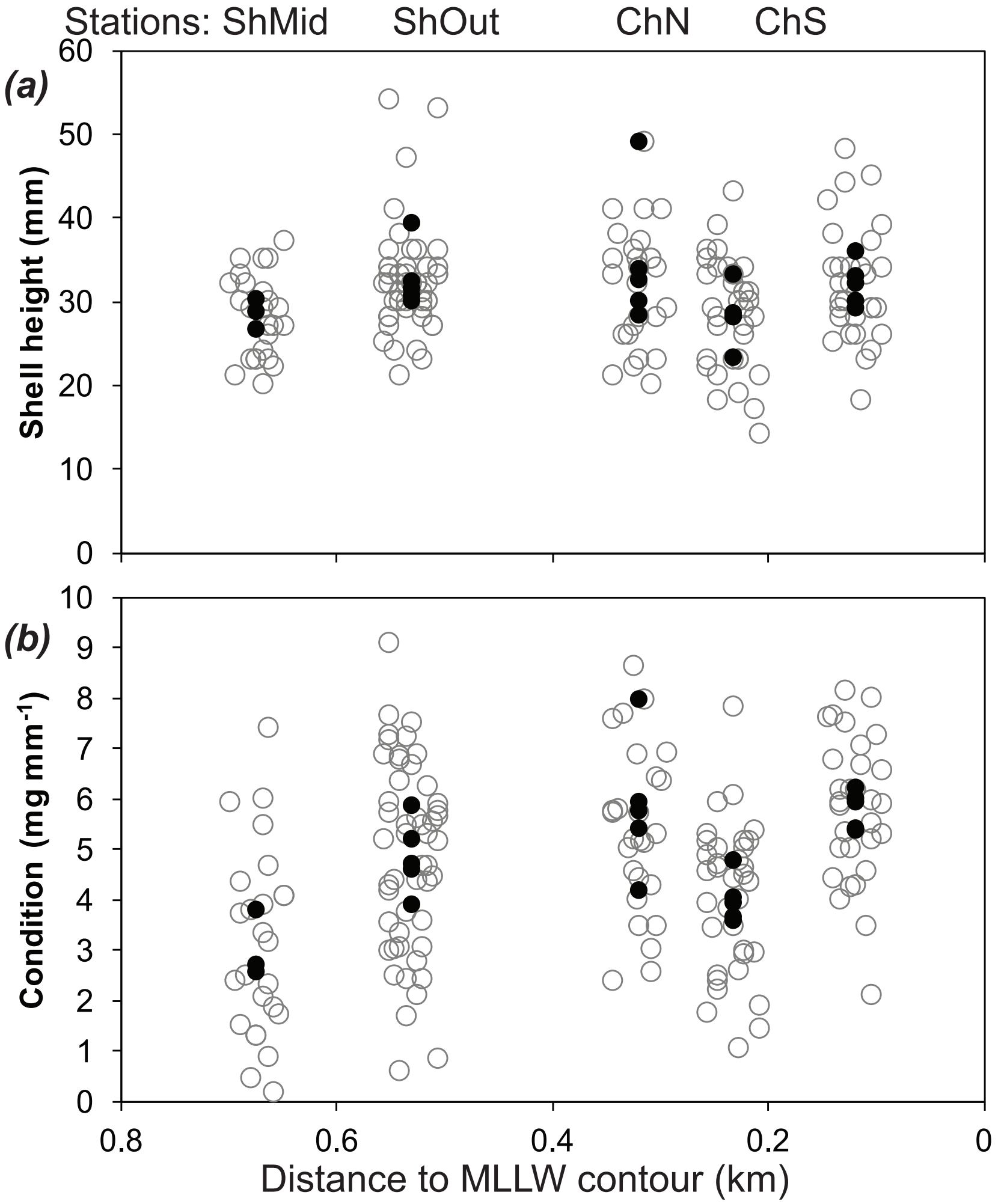
Stations: ShMid
ShOut
ChN
ChS
(a)
Shell height (mm)
60
50
40
30
20
10
0
(b)
Condition (mg mm-1)
10
9
8
7
6
5
4
3
2
1
0
0.8
0.6
0.4
0.2
0
Distance to MLLW contour (km)

Table 1. Comparison of observed and modeled depth-averaged root mean square tidal velocity at six stations in the main channel and intertidal zone of Willapa Bay. Subtidal stations are at depths relative to mean sea level. Intertidal stations are at depths relative to mean high water.

			Depth-averaged rms velocity		
Latitude	Longitude	Water depth	Observed	Model	% error
Subtidal (cf. Banas and Hickey, 2005*)*					
46.694°N	124.097°W	10.1 m (MSL)	0.74 m/s	0.73 m/s	1%
46.697	124.064	10.1	0.78	0.81	4
46.696	123.973	9.75	0.61	0.78	28
46.521	123.999	12.2	0.53	0.63	19
Intertidal (19-28 Jul 2008)					
46.598	124.021	2.1 m (MHW)	0.21 m/s	0.22 m/s	5
46.598	124.031	2.0	0.074	0.10	35

Table 2. Model fit of linear models relating water properties measured from 8 Jun to 28 Aug 2008 at near-channel stations (ChN, ChS in Fig. 3) to coastal upwelling incorporating different lag times. Day of year was included as a predictor variable in all models to account for summer drought and seasonally-increasing salinity in Willapa Bay. Upwelling coefficients are estimates (standard error) from linear models, with significance as *(<0.05), **(<0.01), ***(<0.001). 63 daily values were available for ChN and 68 for ChS.

		Lag in days							
	No upwelling	No lag	1	2	3	4	5	6	7
ChN adjusted r^2	0.617	0.614	0.641	0.669	0.711	**0.713**	0.692	0.685	0.667
ChN Upwelling coefficient		0.004 (0.006)	0.013 (0.006) *	0.018 (0.005) **	0.022 (0.005) ***	0.023 (0.005) ***	0.021 (0.005) ***	0.020 (0.005) ***	0.016 (0.006) **
ChS adjusted r^2	0.633	0.627	0.638	0.660	0.696	**0.728**	0.707	0.688	0.669
ChS Upwelling coefficient		0.0001 (0.006)	0.008 (0.006)	0.014 (0.005) *	0.019 (0.005) ***	0.022 (0.005) ***	0.021 (0.005) ***	0.019 (0.005) ***	0.015 (0.005) **

Table 3. Regression results relating salinity and temperature at shoreward sensors to channel station (ChS) with the most complete time series from 8 Jun to 28 Aug 2008. Model fit is provided as adjusted r^2 for lags of different numbers of tidal cycles. Sample size (N) declines by 3-6 for each lag, due to gaps during sensor cleaning, but results were similar when sample sizes were made equivalent within each sensor comparison. Mean differences come from paired t-tests (relative to ChS) without lags.

		Lagged tidal cycles					
Station	N	No lag	1	2	3	4	Mean difference (95% CI)
Salinity							
ShIn	75	0.947	**0.960**	0.949	0.892	0.837	0.0009 (-0.085, 0.087)
ShMid	103	0.942	**0.947**	0.946	0.936	0.928	-0.241 (-0.367, -0.115)
ShOut	130	**0.972**	0.968	0.956	0.930	0.907	-0.153 (-0.226, -0.080)
Temperature							
ShIn	75	**0.768**	0.083	0.626	0.013	0.486	0.580 (0.450, 0.711)
ShMid	103	**0.865**	0.501	0.735	0.408	0.638	0.622 (0.490, 0.754)
ShOut	130	**0.925**	0.504	0.790	0.407	0.907	0.298 (0.227, 0.369)

Table 4. Results of paired t-tests relating fluorescence at shoreward stations to channel station (ChN) from 2 Aug to 15 Aug 2007. Values for each flood and ebb tide were based on an average of seven values logged at 10-min intervals around the median water level. Mean difference between each sensor and ChN is negative when fluorescence was lower towards shore. Two separate loggers were deployed 50 m apart at the Middle Shore station.

	Flood tides		Ebb tides	
	Mean difference (95% CI)	N	Mean difference (95% CI)	N
ShMid	-6.7 (-8.1, -5.4)	18	-5.0 (-6.3, -3.7)	20
ShMid	-4.2 (-5.9, -2.5)	16	0.0 (-1.7, 1.7)	8
ShOut	-2.7 (-3.9, -1.6)	19	-0.1 (-2.0, 1.8)	13

Supplemental material for Wheat EE, Banas NS, Ruesink JL. 2019. Multi-day water residence time as a mechanism for physical and biological gradients across intertidal flats. Estuarine Coastal and Shelf Science

Table S1. Position of oysters and sensors (YSI 6600) deployed intertidally on a wide tidal flat in Willapa Bay, Washington, USA. Station codes are North Channel (ChN), South Channel (ChS), Outer Shore (ShOut), Middle Shore (ShMid), and Inner Shore (ShIn). Latitude and longitude use WGS84 datum, and UTM uses 10T grid.

Data type	Station	Latitude °N (UTM Northing)	Longitude °W (UTM Easting)	Start date	End date	Elevation m MLLW	Distance to MLLW contour m
Oyster performance	ShMid	46.59702 (5150897)	124.02746 (421302)	3 Aug 2007	19 May 2008	0.6	673
Oyster performance	ShOut	46.59743 (5160940)	124.02550 (421453)	3 Aug 2007	19 May 2008	0.6	530
Oyster performance	ChS	46.59322 (5160469)	124.02153 (421750)	3 Aug 2007	19 May 2008	0.6	118
Oyster performance	ChN	46.59913 (5161126)	124.02274 (421666)	3 Aug 2007	19 May 2008	0.6	318
Oyster performance	ChS	46.59522 (5160695)	124.02618 (421397)	3 Aug 2007	19 May 2008	0.6	231
Salinity, Temperature	ShOut	46.59701 (5160895)	124.02643 (421381)	8 Jun 2008	28 Aug 2008	0.05	600
Salinity, Temperature	ShMid	46.59770 (5160975)	124.03008 (421102)	8 Jun 2008	28 Aug 2008	0.5	880
Salinity, Temperature	ChN	46.59917 (5161129)	124.02123 (421781)	8 Jun 2008	28 Aug 2008	0.6	200
Salinity, Temperature	ShIn	46.60188 (5161444)	124.03427 (420787)	8 Jun 2008	28 Aug 2008	0.9	1200
Salinity, Temperature	ChS	46.59592 (5160770)	124.02272 (421663)	8 Jun 2008	28 Aug 2008	-0.2*	320
Chlorophyll	ShMid	46.59735 (5160937)	124.03089 (421039)	2 Aug 2007	15 Aug 2007	0.7	940
Chlorophyll	ShMid	46.59724 (5160924)	124.03019 (421093)	2 Aug 2007	15 Aug 2007	0.55	890
Chlorophyll	ShOut	46.59637 (5160822)	124.02469 (421513)	2 Aug 2007	15 Aug 2007	0.1	470
Chlorophyll	ChN	46.59811 (5161014)	124.02356 (421602)	2 Aug 2007	15 Aug 2007	-0.1	380

*deployed for the first two weeks at +0.2 m MLLW

Table S2. Estimates for slope and intercept (regression coefficients, with standard error) relating water properties to distance from channel (in km). Six transects were sampled at 5-sec intervals on 17 Aug 2008 to measure surface water with a YSI 6600. N=Number of samples per transect. Intercept is at the start of each transect. Chlorophyll-a (Chl) values were adjusted from sensor fluorescence (0.319) based on calibration by bottle samples. Latitude and longitude use WGS84 datum, and UTM uses 10T grid; both are presented for the start and end of each transect.

Transect	Latitude N (UTM Northing)	Longitude W (UTM Easting)	Chl intercept	Chl slope km^{-1}	Salinity intercept	Salinity slope km^{-1}
1, n=14	46.59559 (5160731)	124.02041 (421840)	4.23 (0.11)	-0.7135 (0.3979)	29.64 (0.021)	-1.05 (0.073)
	46.59596 (5160778)	124.02653 (421372)				
2, n=26	46.59705 (5160893)	124.02017 (421860)	4.12 (0.13)	-2.7345 (0.4185)	29.60 (0.017)	-1.35 (0.058)
	46.59606 (5160790)	124.02665 (421362)				
3, n=20	46.59705 (5160893)	124.02017 (421860)	4.45 (0.14)	-2.755 (0.4600)	29.85 (0.035)	-1.73 (0.118)
	46.59669 (5160860)	124.02768 (421284)				
4, n=27, 19	46.59804 (5161003)	124.02067 (421823)	4.01 (0.15)	-3.974 (0.493)	29.48 (0.020)	-1.60 (0.095)
	46.59705 (5160900)	124.02721 (4212321)				
5, n=23	46.59804 (5161003)	124.02086 (421809)	4.44 (0.15)	-3.469 (0.453)	29.61 (0.017)	-1.32 (0.051)
	46.59744 (5160944)	124.02822 (421244)				
6, n=31	46.59980 (5161199)	124.02056 (421834)	4.17 (0.12)	-4.327 (0.3915)	NA	NA
	46.59752 (5160953)	124.02813 (421251)				